

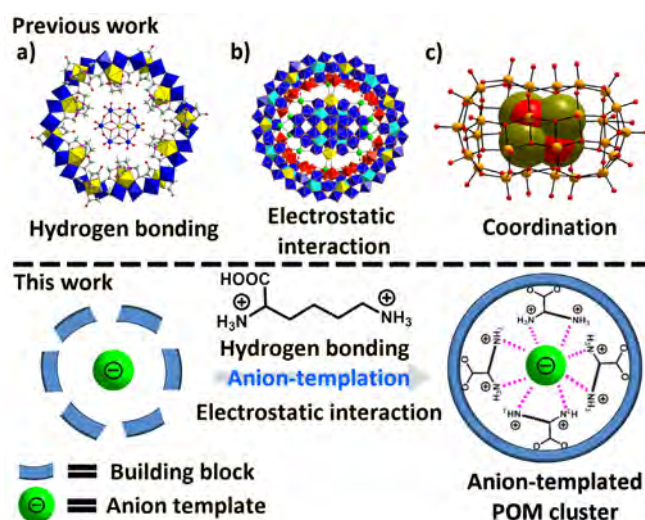
# Unveiling the Key Templates in the Self-Assembly of Gigantic Molybdenum Blue Wheels

Weimin Xuan, Robert Pow, Qi Zheng, Nancy Watfa, De-Liang Long and Leroy Cronin\*

**Abstract:** Template synthesis is a powerful and useful approach to build a variety of functional materials and complicated supramolecular systems. Systematic study on how templates structurally evolve from basic building blocks and then affect the templated self-assembly is critical to understand the underlying mechanism and gain more guidance for designed assembly but remains challenging. Here we describe the templated self-assembly of a series of gigantic Mo Blue (MB) clusters **1-4** using L-ornithine as structure-directing agent. L-ornithine is essential for the formation of such kind of template-host assemblies by providing directional forces of hydrogen bonding and electrostatic interactions. Based on the structural relationship between encapsulated templates of  $\{Mo_8\}$  (**1**),  $\{Mo_{17}\}$  (**2**) and  $\{Mo_{36}\}$  (**4**), a plausible pathway of the structural evolution of templates is proposed, thus giving more insight on the templated self-assembly of Mo Blue clusters.

Template synthesis is not only a versatile approach to fabricate organic chemicals and nanostructured materials but also critical in the self-assembly of functional supramolecular systems.<sup>[1]</sup> Although anion templates are fundamentally important and widely recognized in biological system,<sup>[2]</sup> they are much less explored in synthetic chemistry and supramolecular chemistry, in comparison to cationic and neutral templates, due to their intrinsic diffuse nature, pH sensitivity and relatively higher free energies of solvation.<sup>[3]</sup> In the field of polyoxometalates (POMs)<sup>[4]</sup> - a unique class of anionic discrete metal-oxo clusters with a wide variety of structures and properties, anion templates are essentially for the construction of POM clusters and are generally referred to as heteroanions, such as phosphate, orthoperiodate and phosphite.<sup>[5-7]</sup> Not only do these anions direct the self-assembly of POMs via a templating effect but also affect the resultant structures and thus properties.<sup>[8]</sup> More recently, nanosized POM clusters have been found as anion templates to direct the self-assembly of larger POMs.<sup>[9]</sup> One prominent example is that the intrinsic formation of  $\{Mo_{36}\}$  upon acidification of molybdate allows the self-assembly of the  $\{Mo_{154}\}$  giant Mo Blue wheel, revealing the key role of anionic  $\{Mo_{36}\}$  template.<sup>[9a]</sup> In general, three types of interactions can be established between anionic template and POMs to neutralize the inherent repulsion, i.e., hydrogen bonding,<sup>[9c]</sup> electrostatic interaction<sup>[9a]</sup> and coordination<sup>[9f]</sup> (Scheme 1). In some cases, more than one type of interaction will be observed.<sup>[9d]</sup> Although the templated POM@POM systems have been reported recently,

they are still rare and the underlying mechanism is much less explored. The systematic study of such systems will not only lead to the discovery of completely new clusters based on templated self-assembly and but also provide a chance to gain more insight into the dynamic process during the self-assembly.



**Scheme 1.** Top: representative interactions such as hydrogen bonding, electrostatic interaction and coordination bonds found between anion templates and POM hosts. Bottom: L-ornithine as structure-directing agent during anion-templated self-assembly of Mo Blue clusters via providing both hydrogen bonding (purple dotted line) and electrostatic interaction.

To further extend the POM-templated approach to construct gigantic POMs, we considered that if the interactions mentioned above can be rationally combined, we may be able to build a series of new POM clusters, while elucidating the mechanism of templated self-assembly. In addition, an understanding of the structural evolution of the template species may be derived by trapping fragments/intermediates in larger host structures in different stages of cluster formation. Herein we described the templated self-assembly of a series of Mo Blue wheels **1-4** using L-ornithine as structure directing agent, which provides both electrostatic interaction and hydrogen bonding to stabilize the template-host architecture (Scheme 1). Importantly, the systematic synthetic approach for the formation of **1-4** gives new insight into the structural evolution of the templating species. Compound **1** and **2** share the same framework of  $\{Mo_{150}Ce_2\}$  but with different templates anchored in the center, i.e.,  $\{Mo_{17}\}$  for **1** and  $\{PMo_{12}\}$  for **2**. Compound **3** features a framework of  $\{Mo_{124}Ce_4\}$  with a  $\{Mo_8\}$  cluster located in the middle, while **4** comprises of two wheels  $\{Mo_{154}\}$  and  $\{Mo_{150}\}$ , within the latter of which a  $\{Mo_{36}\}$  template is entrapped. All the compounds were characterized crystallographically and the formula assignments are fully supported using an extensive array of analytical techniques (see SI). Compounds **1-4** can be formulated as:

Dr. W. Xuan, Dr. A. J. Surman, Q. Zheng, Dr. D.-L. Long, Prof. Dr. L. Cronin  
WestCHEM, School of Chemistry, The University of Glasgow  
Glasgow G12 8QQ (UK)  
E-mail: [Lee.Cronin@glasgow.ac.uk](mailto:Lee.Cronin@glasgow.ac.uk)  
Homepage: <http://www.croninlab.com>

Supporting information for this article is given via a link at the end of the document. **(Please delete this text if not appropriate)**

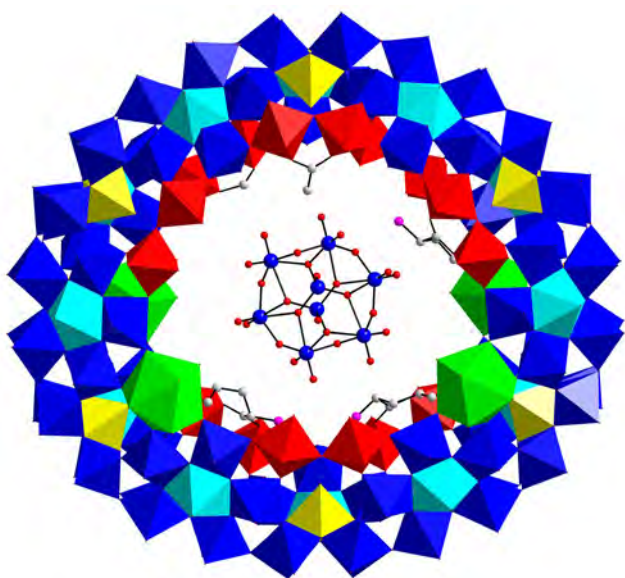
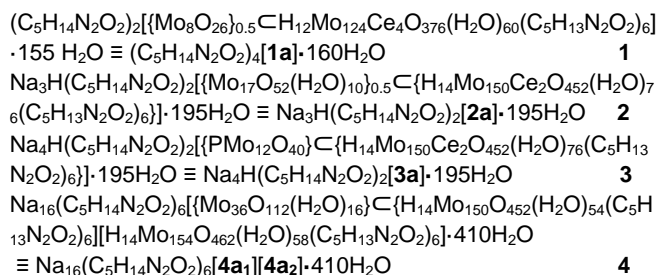


**Figure 1.** View of the Molecular structure of **1a**. The framework of  $\{\text{Mo}_{124}\text{Ce}_4\}$  is presented in polyhedron and the entrapped  $\{\text{Mo}_8\}$  in ball and stick mode.  $\{\text{Mo}_1\}$ , yellow polyhedron;  $\{\text{Mo}_2\}$ , red polyhedron;  $\{\text{Mo}_8\}$ , blue polyhedron with central pentagonal unit in cyan polyhedron; CellI, green polyhedron; C, grey ball; N, pink ball.

Following our previous work in Mo Blue chemistry, L-ornithine was introduced into the synthetic system of lanthanide-doped Mo Blue in a similar procedure (see SI for details),<sup>[10]</sup> to establish whether L-ornithine could assist in trapping an ‘intrinsic’ template that direct the self-assembly. Crucially no preformed anion templates, as established in previous studies, such as the Keggin-type  $\{\text{M}_{12}\}$  or Dawson-type  $\{\text{M}_{18}\}$  were added, yet to our surprise crystals of **1** were obtained in two weeks. Single crystal X-ray structure analysis of **1** reveals a host-guest structure **1a** in which  $\alpha\text{-}[\text{Mo}_8\text{O}_{26}]^{4-}$  ( $\{\text{Mo}_8\}$ ) is encapsulated by  $\{\text{Mo}_{124}\text{Ce}_4\}$  host (Figure 1).<sup>[11]</sup>  $\{\text{Mo}_{124}\text{Ce}_4\}$  is composed of 12  $\{\text{Mo}_8\}$  units, 8  $\{\text{Mo}_2\}$  units, 12  $\{\text{Mo}_1\}$  units and 4  $\{\text{Ce}(\text{H}_2\text{O})_5\}$  units functionalized by L-ornithine ligands on the inner surface. Two  $\text{Ce}^{3+}$  ions are located on the upper rim and separated by one  $\{\text{Mo}_2\}$  unit while another two are situated on the opposite side and separated by two  $\{\text{Mo}_2\}$  units, giving rise to an elliptical wheel. All the L-ornithine ligands are attached onto  $\{\text{Mo}_2\}$  units with the side chain buried in the pitch of  $\{\text{Mo}_{124}\text{Ce}_4\}$ . Due to the limited resolution, only three ornithine can be fully located from the X-ray data.

The  $\{\text{Mo}_8\}$  template locates at the centre of  $\{\text{Mo}_{124}\text{Ce}_4\}$  and is bound by a series of hydrogen bonds formed between terminal O atoms and L-ornithine ligands (Figure S6). In addition, the protonated L-ornithine also acts as charge buffer to reduce repulsive electrostatic force between the anionic  $\{\text{Mo}_8\}$  template and  $\{\text{Mo}_{124}\text{Ce}_4\}$  host. The combination of both hydrogen bonding

and electrostatic interaction is thus believed to be critical to stabilize such kind of template-host architecture.

Under more concentrated condition, decreasing the ratio of  $\text{Ce}^{3+}/\text{MoO}_4^{2-}$  leads to the discovery of compound **2**. Single crystal X-ray structure analysis of **2** reveals a host-guest structure **2a** in which a  $[\text{Mo}_{17}\text{O}_{18}(\text{OH})_6]^{3-}$  ( $\{\text{Mo}_{17}\}$ ) is entrapped by the  $\{\text{Mo}_{150}\text{Ce}_2\}$  host (Figure 2a). The host is isostructural to reported  $\{\text{Mo}_{150}\text{Ce}_2\}$  elliptical ring-shaped structure that is composed of 14  $\{\text{Mo}_8\}$  units, 12  $\{\text{Mo}_2\}$  units, 14  $\{\text{Mo}_1\}$  units and 2  $\{\text{Ce}(\text{H}_2\text{O})_5\}$  units functionalized by six protonated L-ornithine on the inner surface.<sup>[12]</sup> The 2 symmetry-related  $\text{Ce}^{3+}$  ions distribute evenly on the two ends of  $\{\text{Mo}_{150}\text{Ce}_2\}$ , producing an ellipse wheel with outer and inner ring diameter of  $\sim 31$  and  $12 \text{ \AA}$ , respectively, at its most elongated points. The six L-ornithine ligands are grafted onto six  $\{\text{Mo}_2\}$  units via carboxylate groups with the side chain buried in the pitch of  $\{\text{Mo}_{150}\text{Ce}_2\}$  (Figure 2a).

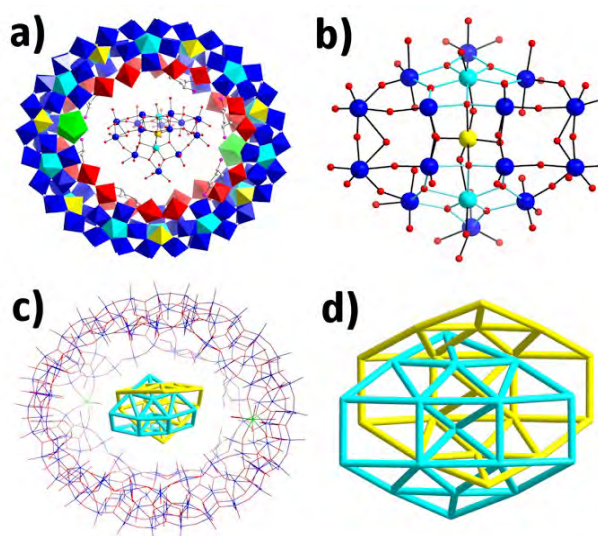


**Figure 2.** a) View of the molecular structure **2a**.  $\{\text{Mo}_{150}\text{Ce}_2\}$  is in polyhedron mode and L-ornithine is in ball and stick model. Color scheme is the same as Figure 1; b) View of the molecular structure of  $\{\text{Mo}_{17}\}$ . The pentagon is highlighted in cyan bonds; c) and d) View of the disordered  $\{\text{Mo}_{17}\}$  in two positions, which are presented in cyan and yellow wire-frames, respectively.

Similar to **1a**, the  $\{\text{Mo}_{17}\}$  template also resides at the centre of  $\{\text{Mo}_{150}\text{Ce}_2\}$  and is anchored in place by a large number of C-H...O hydrogen-bonds formed between terminal O atoms and L-ornithine ligands grafted to the inner surface of the wheel (Figure S7). Moreover, the presence of protonated L-ornithine ligands minimizes the repulsive electrostatic force between the anionic  $\{\text{Mo}_{17}\}$  template and  $\{\text{Mo}_{150}\text{Ce}_2\}$  wheel, thus binding the whole structure together.  $\{\text{Mo}_{17}\}$  is composed of two  $\{\text{Mo}_8\}$  units connected by one  $\{\text{Mo}_1\}$  unit (Figure 2b). The structural motif of  $\{\text{Mo}_{17}\}$  could be related to reported  $\{\text{Mo}_{36}\}$ ,<sup>[13]</sup> which could be simplified as two  $\{\text{Mo}_{17}\}$  joined by two  $\{\text{Mo}_1\}$ . In our previous study,  $\{\text{Mo}_{36}\}$  has been entrapped as transient template during the self-assembly of  $\{\text{Mo}_{154}\}$ <sup>[9a]</sup> and, in this regard,  $\{\text{Mo}_{17}\}$  may be therefore considered as a potential precursor in the formation of the  $\{\text{Mo}_{36}\}$

template. It should be noted that  $\{\text{Mo}_{17}\}$  is disordered equally in two positions within the  $\{\text{Mo}_{150}\text{Ce}_2\}$  host (Figure 2c and 2d).

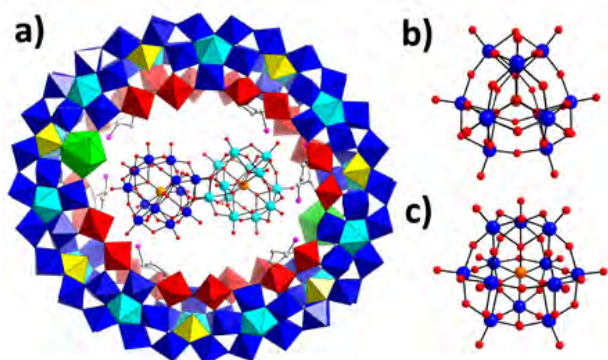


**Figure 3.** a) View of the molecular structure of **3a**. The two parts of disordered  $\{\text{PMo}_{12}\}$  is presented in blue and cyan, respectively; b) and c) Top view and side view of entrapped  $\beta\text{-}\{\text{PMo}_{12}\}$ . Mo – blue, O – red, P – orange.

In our previous work, we have shown that both  $\{\text{PMo}_{12}\}$  and  $\{\text{P}_2\text{W}_{18}\}$  can replace the intrinsic  $\{\text{FeMo}_6\}$  template and direct the aggregation of  $\{\text{Mo}_{24}\text{Fe}_{12}\}$  macrocycle.<sup>[9d]</sup> Given the formation of an intrinsic or 'natural' template in-situ for **2**, we considered whether using a preformed template to induce the formation of  $\{\text{Mo}_{150}\text{Ce}_2\}$  could also be applied here. The addition of preformed  $\{\text{PMo}_{12}\}$  during the synthesis of **2** resulted in the formation of compound **3**. Consistent with **2**, the single crystal X-ray structure analysis of **3** reveals a host-guest structure **3a** where a Keggin-type anion  $\{\text{PMo}_{12}\}$  is bound by the host  $\{\text{Mo}_{150}\text{Ce}_2\}$  (Figure 3a). **3a** is isostructural to **2a** but with the  $\{\text{PMo}_{12}\}$  located in the cavity of  $\{\text{Mo}_{150}\text{Ce}_2\}$ . As such, similar hydrogen bonding patterns and electrostatic interaction are observed as well (Figure S8). Due to the relatively smaller size of  $\{\text{PMo}_{12}\}$  in comparison to the central cavity of  $\{\text{Mo}_{150}\text{Ce}_2\}$ , it is disordered equally on either side of the cavity to maximize the hydrogen bonding and electrostatic interaction. Notably,  $\{\text{PMo}_{12}\}$  adopts  $\beta$ -configuration instead of the  $\alpha$ -isomer (Figure 3b and 3c). This is because  $\beta$ -form is the preferred species under reduced conditions.<sup>[14]</sup>

The templation effect of encapsulated clusters has been studied by *in-situ* by  $^{31}\text{P}$  NMR spectroscopy. Following the synthetic procedure of **3**, a  $^{31}\text{P}$  NMR spectrum was recorded every 10 min after the addition of all starting materials in  $\text{D}_2\text{O}$ . When inadequate  $\{\text{PMo}_{12}\}$  (2.5 mg) was used, which is less than the stoichiometric requirement for the formation of  $\{\text{PMo}_{12}\}\subset\{\text{Mo}_{150}\text{Ce}_2\}$ , signals of  $\{\text{PMo}_{12}\}$  could be detected after 10 min and then completely disappeared after 1 h. In contrast, addition of excess  $\{\text{PMo}_{12}\}$  (8.0 mg) resulted in the presence of peaks of  $\{\text{PMo}_{12}\}$  throughout the reaction process but which became much less intense after 1 h (Figure S11). This indicates that  $\{\text{PMo}_{12}\}$  is a template during the self-assembly, which is gradually consumed upon the formation of  $\{\text{PMo}_{12}\}\subset\{\text{Mo}_{150}\text{Ce}_2\}$  (**3a**). Once  $\{\text{PMo}_{12}\}$  is included as a template, its  $^{31}\text{P}$  NMR signal cannot be observed anymore because of the shielding effect of paramagnetic  $\{\text{Mo}_{150}\text{Ce}_2\}$ . In the case of inadequate template, the  $\{\text{PMo}_{12}\}$  will be completely encapsulated by the host and result in no NMR response of  $\{\text{PMo}_{12}\}$ , while using excessive template results in the presence of signals even after 1 h due to the remaining presence of free  $\{\text{PMo}_{12}\}$  (Figure S10).

The successful encapsulation of  $\{\text{Mo}_8\}$ ,  $\{\text{Mo}_{17}\}$  and  $\{\text{PMo}_{12}\}$  as templates led us to further explore the potential of using L-ornithine as structure-directing agent to entrap different templates, which may in turn give us more insight regarding the formation mechanism of templated self-assembly of Mo Blue clusters. In the cases of **1-3**, lanthanide doped Mo Blue (LMB)  $\{\text{Mo}_{124}\text{Ce}_4\}$  and  $\{\text{Mo}_{150}\text{Ce}_2\}$  provide confined environments to enclose templates. In general, LMB exhibits more curved inner surface and elliptical ring shape and thus smaller size compared with archetype  $\{\text{Mo}_{154}\}$ .<sup>[15]</sup> With this in mind, we performed the synthesis without adding lanthanides to see how the change of curvature and size of MB will affect the entrapped template. After a systematic optimization of the synthetic conditions we were able to obtain another templated MB cluster **4**.

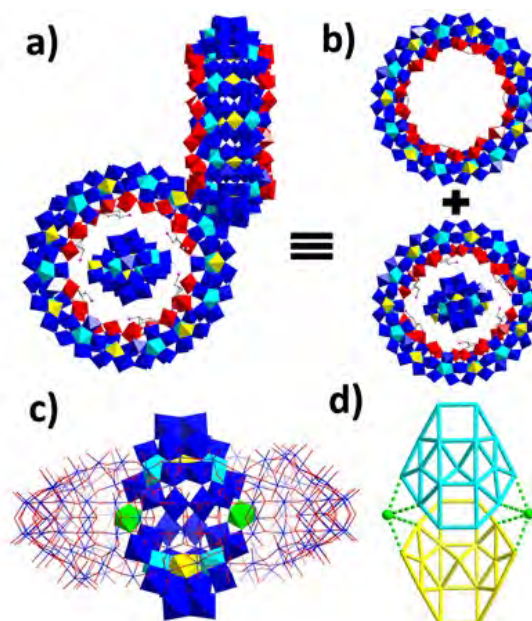
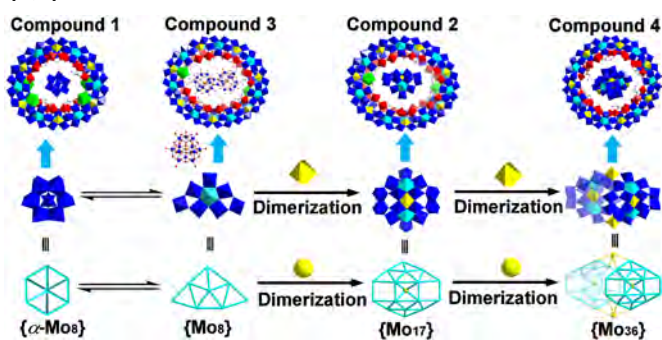


**Figure 4.** a) and b) View of the molecular structure of **4a** consisted of **4a1** and **4a2**; c) Side view of the orientation of  $\{\text{Mo}_{36}\}$  in  $\{\text{Mo}_{150}\}$ .  $\{\text{Mo}_{150}\}$  is in wire-frame mode and two  $\{\text{Mo}_1\}$  units that connect two  $\{\text{Mo}_{17}\}$  are represented in green polyhedra; d) Simplification of  $\{\text{Mo}_{36}\}$  to two  $\{\text{Mo}_{17}\}$  (cyan and yellow wires) linked by two  $\{\text{Mo}_1\}$  (green ball).

Single-crystal X-ray structure analysis reveals that **4** crystallizes in space group  $P-1$  and consists of two crystallographically independent wheels in the molecular structure, denoted as **4a1** and **4a2**, respectively (Figure 4a and 4b). **4a1** features a host-guest architecture that a  $[\text{Mo}_{36}\text{O}_{112}(\text{H}_2\text{O})_{16}]^{8-}$  ( $\{\text{Mo}_{36}\}$ ) is entrapped by the  $\{\text{Mo}_{150}\}$  host. The  $\{\text{Mo}_{150}\}$  adopts the same framework of archetypal  $\{\text{Mo}_{154}\}$  that is constructed from 14 sets of  $\{\text{Mo}_{11}\}$  units but with two  $\{\text{Mo}_2\}$  defect sites on the rim of the wheel (Figure 4b).<sup>[15a]</sup> The  $\{\text{Mo}_{36}\}$ , which is situated in the center of the  $\{\text{Mo}_{150}\}$  cavity, is structurally equivalent to the well-known and previously described  $\{\text{Mo}_{36}\}$ ,<sup>[13]</sup> as observed in the reported  $\{\text{Mo}_{36}\}\subset\{\text{Mo}_{150}\}$ .<sup>[9a]</sup> There are also six L-ornithine attached on six  $\{\text{Mo}_2\}$  units in **4a1**. Among them, two pairs of L-ornithine are orientated in tail-to-tail mode with the terminal amino groups pointing to each other while the remaining two arrange freely.<sup>[10]</sup> Similar to **1-3**, positively charged L-ornithine ligands not only serve as buffer charge to glue the anionic  $\{\text{Mo}_{36}\}$  template and  $\{\text{Mo}_{150}\}$

host together but also form a multiplicity of hydrogen bonding with both the terminal and bridging O atoms on  $\{Mo_{36}\}$ , to further stabilize the aggregate (Figure S9). In addition, several sodium ions are also found between  $\{Mo_{36}\}$  and  $\{Mo_{150}\}$ . Notably,  $\{Mo_{36}\}$  in the reported  $\{Mo_{36}\} \subset \{Mo_{150}\}$  retains a parallel orientation along with  $\{Mo_{150}\}$  and is thus completely entrapped within the cavity of  $\{Mo_{150}\}$  (Figure S10).<sup>[9a]</sup> However,  $\{Mo_{36}\}$  in **4a<sub>1</sub>** adopts a vertical orientation that is almost perpendicular to the plane defined by  $\{Mo_{150}\}$ , with the two rims stretching out of  $\{Mo_{150}\}$  (Figure 4c). This is caused by the concomitant accommodation of six L-ornithine in **4a<sub>1</sub>** along with  $\{Mo_{36}\}$ , which reduces the available space to fully encompass  $\{Mo_{36}\}$  and thus force it rotate along its lateral axis, resulting in the  $\{Mo_{36}\}$  extending out beyond either side of the  $\{Mo_{150}\}$  cavity.

**4a<sub>2</sub>** adopts the same framework as  $\{Mo_{154}\}$  with L-ornithine functionalized on the inner surface. Due to the limited resolution of crystal data, only carboxylate group of the L-ornithine could be identified. Although the central cavity of **4a<sub>2</sub>** is large enough to accommodate  $\{Mo_{36}\}$ , no template is found in the cavity of **4a<sub>2</sub>**. From the space filling modes of **4a<sub>1</sub>**, **4a<sub>2</sub>** and  $\{Mo_{36}\} \subset \{Mo_{150}\}$ , it can be seen that  $\{Mo_{150}\}$  host in **4a<sub>1</sub>** and  $\{Mo_{36}\} \subset \{Mo_{150}\}$  exhibit slightly elliptical ring due to the symmetric defect of two  $\{Mo_2\}$  units at the two elongated ends, while **4a<sub>2</sub>** adopts roughly regular ring as exhibited by the archetypal  $\{Mo_{154}\}$  (Figure S10). Taking account of the space occupied by L-ornithine and the size and shape of  $\{Mo_{36}\}$  (1.4 nm x 1.6 nm x 2.1 nm), this kind of arrangement makes  $\{Mo_{150}\}$  can either accommodate  $\{Mo_{36}\}$  along its lateral axis (**4a<sub>1</sub>**) or longitudinal axis ( $\{Mo_{36}\} \subset \{Mo_{150}\}$ ). In contrast, the cavity of **4a<sub>2</sub>** is too large in comparison to  $\{Mo_{36}\}$  and thus is unable to capture  $\{Mo_{36}\}$  efficiently. The encapsulation of  $\{Mo_{36}\}$  in **4a<sub>1</sub>** further confirms that  $\{Mo_{36}\}$  is a key template during the self-assembly of Mo Blue, consistent with our previous study.<sup>[9a,9b]</sup>



**Scheme 2.** The anion-templated self-assembly of macrocycles **1-4** and transformation from **1** to **2** and **3** by template-exchange.

The formation of compounds **1-4** with L-ornithine as structure-directing agent allows us to propose a potential mechanism of templated self-assembly underpinning the formation of the compounds **1-4** (Scheme 2). The process could be described as follow: Firstly, the basic building blocks of  $\{Mo_8\}$ ,  $\{Mo_2\}$  and  $\{Mo_1\}$  form in solution. Next, the labile  $\{Mo_8\}$  could either transform to isomeric  $\alpha\text{-}\{Mo_8\}$  or dimerize with one  $\{Mo_1\}$  to generate  $\{Mo_{17}\}$  *in-situ*, which then behave as templates to drive the self-assembly of **1** and **2** under the direction of L-ornithine, respectively. If the preformed  $\{PMo_{12}\}$  is introduced during the synthesis of **2**, then the initiation of  $\{Mo_{17}\}$  is prevented and **3** will be constructed with  $\{PMo_{12}\}$  as templating species. The dimerization of  $\{Mo_{17}\}$  to form

$\{Mo_{36}\}$  presents a new template that can direct the formation of **4a<sub>1</sub>** together with L-ornithine.

In summary, we describe anion-templated self-assembly of MB clusters **1-4** featuring template $\subset$ host architectures with L-ornithine as structure-directing agent. Upon protonation, L-ornithine not only serves as charge buffer to bind the anionic templates and hosts together, but also provides hydrogen bonding sites to strongly interact with templates, which is believed to be essential for the formation of **1-4**. The successful construction of **1** unveils the ‘intrinsic template’ of  $\{Mo_8\}$  formed *in-situ*. Under more concentrated conditions,  $\{Mo_{17}\}$  is entrapped as a template to induce the self-assembly of **2**, which could be replaced by the preformed  $\{PMo_{12}\}$ , leading to the formation of **3**. <sup>31</sup>P NMR study during the synthesis of **3** illustrates the self-assembly is essentially template-dependent. Moreover, the encapsulation of  $\{Mo_{36}\}$  in **4a<sub>1</sub>** further confirms that  $\{Mo_{36}\}$  is a key template during the self-assembly of Mo Blue clusters. Due to the structural relationship between  $\{Mo_8\}$ ,  $\{Mo_{17}\}$  and  $\{Mo_{36}\}$ , it is reasonable to assume that  $\{Mo_{36}\}$  may be constructed via dimerization of  $\{Mo_{17}\}$ , which itself can be built from dimerization of  $\{Mo_8\}$ , showing a potential stepwise pathway for template assembly in solution. Based on these observations, the formation mechanism for these host-guest aggregates is proposed. In the future, we will further explore the concept of templated synthesis in POM chemistry and study the underlying principles of self-assembly as well.

## Acknowledgements

This work was supported by the EPSRC grants (No. EP/J015156/1; EP/L023652/1; EP/I033459/1; EP/J015156/1; EP/K023004/1; EP/L023652/1), EC grant 318671 MICREAGENTS, LC thanks the Royal Society / Wolfson Foundation for a Merit Award and the ERC for an Advanced Grant (ERC-ADG, 670467 SMART-POM). We thank the Diamond Light Source for time on Beamline I19 under the proposal MT16085.

**Keywords:** gigantic cluster • anion templation • polyoxometalates • molybdenum blue • host-guest chemistry

- [1] a) O. Costisor, W. Linert, *Metal Mediated Template Synthesis of Ligands*, World Scientific Publishing, Singapore, **2004**; b) N.V.Gerbeleu, V. B. Arion, J. P. Burgess, *Template Synthesis of Macrocyclic Compounds*, Wiley-VCH, Weinheim, **1999**; c) C. A. Schalley, F. Vçgtle, K. H. Dçtz, *Templates in Chemistry*, Springer, Berlin, **2005**; d) P. Stang, F. Diederich, *Templated Organic Synthesis*, Wiley-VCH, Weinheim, **2000**; e) Y. Liu, J. Goebel, Y. Yin, *Chem. Soc. Rev.* **2013**, *42*, 2610–2653; f) C. Liang, Z. Li, S. Dai, *Angew. Chem. Int. Ed.* **2008**, *47*, 3696–3717; *Angew. Chem.* **2008**, *120*, 3754–3776.
- [2] a) C. H. Henkels, J. C. Kurz, C. A. Fierke, T. G. Oas, *Biochemistry* **2001**, *40*, 2777–2789; b) M. J. Langton, C. J. Serpell, P. D. Beer, *Angew. Chem. Int. Ed.* **2016**, *55*, 1974–1987; *Angew. Chem.* **2016**, *128*, 2012–2026; c) H. Barber-Brygoo, A. D. Angeli, S. Filleur, J.-M Frachisse, F. Gambale, S. Thomine, S. Wege, *Annu. Rev. Plant Biol.* **2011**, *62*, 25–51; d) J. L. Sessler, P. A. Gale, W.-S. Cho, *Anion Receptor Chemistry*, Royal Society of Chemistry, Cambridge, **2006**; e) P. Chakrabarti, *J. Mol. Biol.* **1993**, *234*, 463–482.
- [3] a) M. S. Vickers and P. D. Beer, *Chem. Soc. Rev.*, **2007**, *36*, 211–225; b) N. Gimeno, R. Vilar, *Coord. Chem. Rev.* **2006**, *250*, 3161–3189; c) A. Bianchi, K. Bowman-James, E. Garcia-España (Eds.), *Supramolecular Chemistry of Anions*, Wiley-VCH, New York, **1997**; d) P. A. Gale, T. Gunlaugson (Eds.), *Themed issue: supramolecular chemistry of anionic species*, *Chem. Soc. Rev.* **2010**, *39*, 3581–4008; e) P. D. Beer, P. A.

- Gale, *Angew. Chem. Int. Ed.* **2001**, *40*, 486-516; *Angew. Chem.* **2001**, *113*, 502-532.
- [4] a) L. Cronin, A. Müller (Eds.), *Themed issue: polyoxometalate cluster science*, *Chem. Soc. Rev.* **2012**, *41*, 7325-7648; b) D.-L. Long, E. Burkholder, L. Cronin, *Chem. Soc. Rev.* **2007**, *36*, 105-121; c) D.-L. Long, R. Tsunashima, L. Cronin, *Angew. Chem. Int. Ed.* **2010**, *49*, 1736-1758; *Angew. Chem.* **2010**, *122*, 1780-1803; d) D.-Y. Du, L.-K. Yan, Z.-M. Su, S.-L. Li, Y.-Q. Lan, E.-B. Wang, *Coord. Chem. Rev.* **2013**, *257*, 702-717. e) M. T. Pope, A. Müller, *Polyoxometalate Chemistry: From Topology via Self-Assembly to Applications*, Kluwer, Dordrecht, **2001**; f) C. L. Hill, (Eds.), *Special issue on polyoxometalate*, *Chem. Rev.* **1998**, *98*, 1-390; g) A. Dolbecq, E. Dumas, C. R. Mayer, P. Mialane, *Chem. Rev.* **2010**, *110*, 6009-6048; h) S.-S. Wang, G.-Y. Yang, *Chem. Rev.* **2015**, *115*, 4893-4962; i) K. Kamata, K. Yonehara, Y. Sumida, K. Yamaguchi, S. Hikichi, N. Mizuno, *Science*, **2003**, *300*, 964-966; j) B. Rausch, M. D. Symes, G. Chisholm, L. Cronin, *Science*, **2014**, *345*, 1326-1330; k) C. Busche, L. Vilà-Nadal, J. Yan, H. N. Miras, D.-L. Long, V. P. Georgiev, A. Asenov, R. H. Pedersen, N. Gadegaard, M. M. Mirza, D. J. Paul, J. M. Poblet, L. Cronin, *Nature*, **2014**, *515*, 545-549; l) M. Shiddiq, D. Komijani, Y. Duan, A. Gaita-Ariño, E. Coronado, S. Hill, *Nature*, **2016**, *531*, 348-351.
- [5] a) J. F. Keggin, *Nature* **1933**, *131*, 908-909; b) B. Dawson, *Acta Crystallogr. Sect. B* **1953**, *6*, 113-126; c) R. Strandberg, *Acta Chem. Scand. Ser. A* **1975**, *29*, 350-358.
- [6] a) D.-L. Long, Y. F. Song, E. F. Wilson, P. Kögerler, S. X. Guo, A. M. Bond, J. S. J. Hargreaves, L. Cronin, *Angew. Chem. Int. Ed.* **2008**, *47*, 4384-4387; *Angew. Chem.* **2008**, *120*, 4456-4459; b) L. Vilà-Nadal, K. Peuntinger, C. Busche, J. Yan, D. Lüders, D.-L. Long, J. M. Poblet, D. M. Guldi, L. Cronin, *Angew. Chem. Int. Ed.* **2013**, *52*, 9695-9699; *Angew. Chem.* **2013**, *125*, 9877-9881.
- [7] a) Q. Zheng, L. Vilà-Nadal, C. Busche, J. S. Mathieson, D.-L. Long, L. Cronin, *Angew. Chem. Int. Ed.* **2015**, *54*, 7895-7899; *Angew. Chem.* **2015**, *127*, 8006-8010; b) U. Kortz, J. Vaissermann, R. Thouvenot, P. Gouzerh, *Inorg. Chem.* **2003**, *42*, 1135-1139.
- [8] a) M. T. Pope, *Heteropoly and Isopoly Oxometalates*, Springer-Verlag, Berlin, **1983**; b) J. B. Moffat, *Metal-Oxygen Clusters: The Surface and Catalytic Properties of Heteropoly Oxometalates*, Springer, New York, **2001**. c) X. López, J. J. Carbó, C. Bo, J. M. Poblet, *Chem. Soc. Rev.* **2012**, *41*, 7537-7571; d) T. Ueda, *ChemElectroChem*, **2018**, *5*, 823-838; e) Q. Zheng, L. Vilà-Nadal, Z. Lang, J.-J. Chen, D.-L. Long, J. S. Mathieson, J. M. Poblet, L. Cronin, *J. Am. Chem. Soc.* **2018**, *140*, 2595-2601; f) J. Yan, D.-L. Long, E. F. Wilson, L. Cronin, *Angew. Chem. Int. Ed.* **2009**, *48*, 4376-4380; *Angew. Chem.* **2009**, *121*, 4440-4444; g) U. Kortz, M. G. Savelieff, F. Y. A. Ghali, L. M. Khalil, S. A. Maalouf, D. I. Sinno, *Angew. Chem. Int. Ed.* **2002**, *41*, 4070-4073; *Angew. Chem.* **2002**, *114*, 4246-4249.
- [9] a) H. N. Miras, G. J. T. Cooper, D.-L. Long, H. Bögge, A. Müller, C. Streb, L. Cronin, *Science* **2010**, *327*, 72-74; b) H. N. Miras, C. J. Richmond, D.-L. Long, L. Cronin, *J. Am. Chem. Soc.* **2012**, *134*, 3816-3824; c) X. Fang, L. Hansen, F. Haso, P. Yin, A. Pandey, L. Engelhardt, I. Slowing, T. Li, T. Liu, M. Luban, D. C. Johnston, *Angew. Chem. Int. Ed.* **2013**, *52*, 10500-10504; *Angew. Chem.* **2013**, *125*, 10694-10698; d) W. Xuan, R. Pow, D.-L. Long, L. Cronin, *Angew. Chem. Int. Ed.* **2016**, *55*, 12703-12707; *Angew. Chem.* **2016**, *128*, 12895-12899; e) A. Müller, S. K. Das, P. Kögerler, H. Bögge, M. Schmidtman, A. X. Trautwein, V.

## SUPPLEMENTARY INFORMATION

---

### Unveiling the Key Templates in the Self-assembly of Gigantic Molybdenum Blue Wheels

Weimin Xuan, Robert Pow, Qi Zheng, Nancy Watfa, De-Liang Long and Leroy Cronin\*

WestCHEM, School of Chemistry, The University of Glasgow, University Avenue, Glasgow G12 8QQ, Scotland, UK; Fax: (+44)-141-330-4888;

E-mail: [lee.cronin@glasgow.ac.uk](mailto:lee.cronin@glasgow.ac.uk);

Homepage: <http://www.croninlab.com>

### Table of Contents

1. Materials	S2
2. Instrumentation	S2
3. Synthetic procedure of <b>1-4</b>	S3
4. Structure analysis of <b>1-4</b>	S4
5. Crystallographic data and crystal structures of <b>1-4</b>	S9
6. References	S13

## 1. Materials

Reagent-grade chemicals were obtained from Aldrich Chemical Company Ltd. and Alfa Aesar, and used without further purification.

## 2. Instrumentation

**Crystallography:** Suitable single crystal was selected and mounted onto a rubber loop using Fomblin oil. X-ray diffraction intensity data a Bruker Apex 2 CCD diffractometer ( $\lambda$  (MoK $\alpha$ ) = 0.7107 Å) equipped with a microfocus x-ray source (50kV, 30w). Data collection and reduction were performed using the Apex2 software package and structure solution, and refinement were carried out using SHELXS-2016<sup>[1]</sup> and SHELXL-2016<sup>[2]</sup> using WinGX.<sup>[3]</sup> Corrections for incident and diffracted beam absorption effects were applied using empirical absorption correction. All the Mo atoms (including those disordered) and most of the O atoms were refined anisotropically. Solvent water molecule sites with partial occupancy were found and included in the structure refinement. Crystallographic formulas typically contain much more water molecules in the crystal lattice than the formulas used for chemical analyses as the sample was dried up. It is important to note that with these structures we are moving outside the realm of small molecule crystallography and are dealing with refinements and problems that lie between small molecule and protein crystallography. As a result we cannot expect refinements and statistics to follow the path of crystals with much smaller unit cells. However, the final refinement statistics are relatively good, and in all cases the structural analysis allows us to unambiguously fully determine the structures of the compounds. The X-ray crystallographic data reported in this article have been deposited at the Crystallographic Data Centres. For compound **1**, the data can be obtained free of charge from the Cambridge Crystallographic Data Centre via [www.ccdc.cam.ac.uk/data\\_request/cif](http://www.ccdc.cam.ac.uk/data_request/cif) under deposition number CCDC-1874914-1874917.

**Fourier-transform infrared (FT-IR) spectroscopy:** The samples were prepared as a KBr pellet and the FT-IR spectrum was collected in transmission mode in the range of 600-4000 cm<sup>-1</sup> using a JASCO FT-IR 4100 spectrometer. Wavenumbers are given in cm<sup>-1</sup>. Intensities are denoted as w = weak, m = medium, s = strong, br = broad, sh = sharp.

**Element Analyses:** Element analyses for Mo, Ce, K and Na were performed on a Leeman inductivity-coupled plasma (ICP) spectrometer while C, N and H content were determined by the microanalysis services within the Department of Chemistry, University of Glasgow using an EA 1110 CHNS, CE-440 Elemental Analyzer.

**Thermogravimetric Analysis (TGA):** Thermogravimetric analysis was performed on a TA Instruments Q 500 Thermogravimetric Analyzer under nitrogen flow at a typical heating rate of 10°C min<sup>-1</sup>.

**<sup>31</sup>P Nuclear Magnetic Resonance Spectroscopy:** <sup>31</sup>P NMR spectroscopy was recorded on a Bruker DPX 500 spectrometer. All samples were prepared by dissolving the clusters in D<sub>2</sub>O or performing the reaction directly in D<sub>2</sub>O.

### 3. Synthetic procedure of 1-4

**1:** (C<sub>5</sub>H<sub>14</sub>N<sub>2</sub>O<sub>2</sub>)<sub>2</sub>[H<sub>12</sub>Mo<sub>128</sub>Ce<sub>4</sub>O<sub>389</sub>(H<sub>2</sub>O)<sub>60</sub>(C<sub>5</sub>H<sub>13</sub>N<sub>2</sub>O<sub>2</sub>)<sub>6</sub>]·160 H<sub>2</sub>O, M.W.: 24107.35

L-ornithine.HCl (6.5 mg, 0.04 mmol), CeCl<sub>3</sub>·7H<sub>2</sub>O (37.3 mg, 0.1 mmol) and N<sub>2</sub>H<sub>4</sub>·2HCl (4.2 mg, 0.04 mmol) were added to a solution of Na<sub>2</sub>MoO<sub>4</sub>·2H<sub>2</sub>O (242 mg, 1 mmol) in water (45 mL). The mixture was then acidified with 1M HClO<sub>4</sub> (4.5 mL). After heating with medium stirring in a 100-mL Erlenmeyer flask (widenecked; covered with a watch glass) at 90 °C for 1 h, the resulting clear deep-blue solution was then cooled to room temperature, filtered and kept in an open 100-mL Erlenmeyer flask for 3 weeks. The deep-blue crystals were collected by filtration, washed with ice-cold H<sub>2</sub>O, and dried under inert atmosphere over CaCl<sub>2</sub>, yield: 35 mg (18.6 % based on Mo). Elemental analysis, calc.: C, 1.99 %; H, 2.33 %; N, 0.93 %; Na, 0 %; Mo, 50.94 %, Ce, 2.32 %; found: C, 2.17 %; H, 1.79 %; N, 0.91 %; Na, 0.08 %; Mo, 50.29 %; Ce, 2.59 %. IR (KBr pellet, 4000–600 cm<sup>-1</sup>): 3386 (s, br), 3180 (s, br), 2922 (w), 2852 (w), 1730 (w), 1608 (s), 1492 (w), 1430 (w), 1350 (w), 967 (m; ν (Mo=O)), 871(m), 801(s), 634 (s), 554 (s).

**2:** Na<sub>3</sub>(C<sub>5</sub>H<sub>14</sub>N<sub>2</sub>O<sub>2</sub>)<sub>2</sub>[H<sub>14</sub>Mo<sub>158.5</sub>Ce<sub>2</sub>O<sub>478</sub>(H<sub>2</sub>O)<sub>81</sub>(C<sub>5</sub>H<sub>13</sub>N<sub>2</sub>O<sub>2</sub>)<sub>6</sub>]·195H<sub>2</sub>O, M.W.: 29257.07

L-ornithine.HCl (28.6 mg, 0.17 mmol), CeCl<sub>3</sub>·7H<sub>2</sub>O (75 mg, 0.2 mmol) and N<sub>2</sub>H<sub>4</sub>·2HCl (15 mg, 0.14 mmol) were added to a solution of Na<sub>2</sub>MoO<sub>4</sub>·2H<sub>2</sub>O (1 g, 4.13 mmol) in water (70 mL). The mixture was then acidified with concentrated HCl to pH ~1.0. After heating with medium stirring in a 100-mL Erlenmeyer flask (widenecked; covered with a watch glass) at 90 °C for 1 h, the resulting clear deep-blue solution was then cooled to room temperature, filtered and kept in an open 100-mL Erlenmeyer flask for 1 week. The deep-blue crystals were collected by filtration, washed with ice-cold H<sub>2</sub>O, and dried under inert atmosphere over CaCl<sub>2</sub>, yield: 275 mg (36.4 % based on Mo). Elemental analysis, calc.: C, 1.64 %; H, 2.32 %; N, 0.77 %; Na, 0.24 %; Mo, 51.98 %, Ce, 0.93%; found: C, 1.66 %; H, 1.66 %; N, 0.72 %; Na, 0.20 %; Mo,

51.70 %; Ce, 1.05 %. IR (KBr pellet, 4000–600  $\text{cm}^{-1}$ ): 3396 (s, br), 3184 (s, br), 2921 (w), 2853 (w), 1735 (w), 1611 (s), 1497 (W), 1425 (2), 1341 (W), 968 (m;  $\nu$  (Mo=O)), 764 (s), 650 (s), 554 (s).

**3:**  $\text{Na}_4\text{H}(\text{C}_5\text{H}_{14}\text{N}_2\text{O}_2)_2[\text{H}_{14}\text{Mo}_{162}\text{Ce}_2\text{PO}_{492}(\text{H}_2\text{O})_{76}(\text{C}_5\text{H}_{13}\text{N}_2\text{O}_2)_6]\cdot 195\text{H}_2\text{O}$ , M.W.: 29781.75

L-ornithine.HCl (28.6 mg, 0.17 mmol),  $\text{CeCl}_3\cdot 7\text{H}_2\text{O}$  (75 mg, 0.2 mmol),  $\text{H}_3\text{PMo}_{12}\text{O}_{40}\cdot n\text{H}_2\text{O}$  (80 mg, 0.044 mmol) and  $\text{N}_2\text{H}_4\cdot 2\text{HCl}$  (15 mg, 0.14 mmol) were added to a solution of  $\text{Na}_2\text{MoO}_4\cdot 2\text{H}_2\text{O}$  (1 g, 4.13 mmol) in water (70 mL). The mixture was then acidified with concentrated HCl to pH ~1.0. After heating with medium stirring in a 100-mL Erlenmeyer flask (widenecked; covered with a watch glass) at 90 °C for 1 h, the resulting clear deep-blue solution was then cooled to room temperature, filtered and kept in an open 100-mL Erlenmeyer flask for 1 week. The deep-blue block-like crystals were collected by filtration, washed with ice-cold  $\text{H}_2\text{O}$ , and dried under inert atmosphere over  $\text{CaCl}_2$ , yield: 256 mg (31.2 % based on Mo). Elemental analysis, calc.: C, 1.61 %; H, 2.24 %; N, 0.75 %; Na, 0.31 %; Mo, 52.19 %; Ce, 0.94 %; P, 0.10 %; found: C, 1.62 %; H, 1.59 %; N, 0.70 %; Na, 0.30 %; Mo, 52.40 %; Ce, 1.08 %; P, 0.16 %. IR (KBr pellet, 4000–600  $\text{cm}^{-1}$ ): 3376 (s, br), 3174 (s, br), 2921 (w), 2852 (w), 1607 (s), 1492 (w), 1432 (w), 1350 (w), 967 (m;  $\nu$  (Mo=O)), 867(m), 766(s), 634 (s), 554 (s).

**4:**  $\text{Na}_{16}(\text{C}_5\text{H}_{14}\text{N}_2\text{O}_2)_6[\text{H}_{28}\text{Mo}_{340}\text{O}_{1026}(\text{H}_2\text{O})_{128}(\text{C}_5\text{H}_{13}\text{N}_2\text{O}_2)_{12}]\cdot 410\text{H}_2\text{O}$ , M.W.: 61526.30

L-ornithine.HCl (67.5 mg, 0.40 mmol) and  $\text{N}_2\text{H}_4\cdot 2\text{HCl}$  (16 mg, 0.15 mmol) were added to a solution of  $\text{Na}_2\text{MoO}_4\cdot 2\text{H}_2\text{O}$  (3 g, 12.39 mmol) in water (100 mL). The mixture was then acidified with concentrated HCl to pH ~1.2. After heating with medium stirring in a 100-mL Erlenmeyer flask (widenecked; covered with a watch glass) at 90 °C for 1 h, the resulting clear deep-blue solution was then cooled to room temperature, filtered the next day to remove crystalline precipitate and kept in an open 100-mL Erlenmeyer flask for 2 weeks. The deep-blue block-like crystals were collected by filtration, washed with ice-cold  $\text{H}_2\text{O}$ , and dried under inert atmosphere over  $\text{CaCl}_2$ , yield: 260 mg (11.5 % based on Mo). Elemental analysis, calc.: C, 1.76 %; H, 2.20 %; N, 0.82 %; Na, 0.60 %; Mo, 53.02 %; found: C, 1.88 %; H, 1.62 %; N, 0.82 %; Na, 0.58 %; Mo, 51.95 %. IR (KBr pellet, 4000–600  $\text{cm}^{-1}$ ): 3409 (s, br), 3223 (s, br), 2923 (w), 2853 (w), 1610 (s), 1493 (w), 1437 (w), 1348 (w), 971 (m;  $\nu$  (Mo=O)), 882(m), 785(s), 635 (s), 556 (s).

#### 4. Structural analysis of 1-4

Although the wheel-type molybdenum blue architectures are very complex, the general approach to the structural analysis and formula determination is well documented.<sup>[4]</sup> The structural analysis requires the following lines of evidence / information to allow the assignment of formula and the structural details coupled with Single-crystal X-ray diffraction:

- (i) Redox titration to help determine the number of reduced Mo<sup>V</sup> centres (UV-vis-NIR spectroscopy also can help corroborate this data via the analysis of the extinction coefficient for the LMCT associated with the reduced Mo<sup>V</sup> centres. Each centre should contribute ca.  $5 - 6 \times 10^3 \text{ L mol}^{-1} \cdot \text{cm}^{-1}$  to  $\epsilon$ ).
- (ii) Bond valence sum analysis to confirm the terminal oxo positions, reduced Mo<sup>V</sup> centres and the positions of the hydroxide ligands.<sup>[5]</sup>
- (iii) Elemental analysis of sodium, molybdenum, cerium and C, H, N analysis.
- (iv) TGA to estimate the number of ligand and solvent water molecules.

Therefore, the analysis below both presents this data and demonstrates how the structural assignment is consistent with this data.

#### Redox titrations

Because of the rather poor solubility of compounds **1-4**, it is not possible to perform redox titration measurements to determine the number of reduced metal centers present.

#### Bond valence sum analysis

**Table S1.** Average bond valence sum values for the Mo centres which span the incomplete {Mo<sub>5</sub>O<sub>6</sub>}-type double cubanes and the  $\mu_3$ -O atoms of the  $\{(\mu_3\text{-O})_2\text{O}_2\}$ -type compartments in **1-4**.

Compounds	BVS (Mo)	BVS ( $\mu_3$ -O)
<b>1</b>	5.71	1.25
<b>2</b>	5.59	1.23
<b>3</b>	5.58	1.27
<b>4</b>	5.56	1.21

## Elemental analysis and C, H, N analysis

See Section 3. Synthetic procedure of **1-4**

## Uv-vis-NIR spectra and TGA curves

Because of the rather poor solubility of compounds **1-4**, we could not prepare the related solution with accurate concentration. Therefore, the Uv-vis spectra of **1-4** were recorded in saturated aqueous solution and  $\epsilon$  was not calculated. All the Uv-vis spectra of **1-4** show the characteristic band of Mo Blue which is centered around 745 nm.

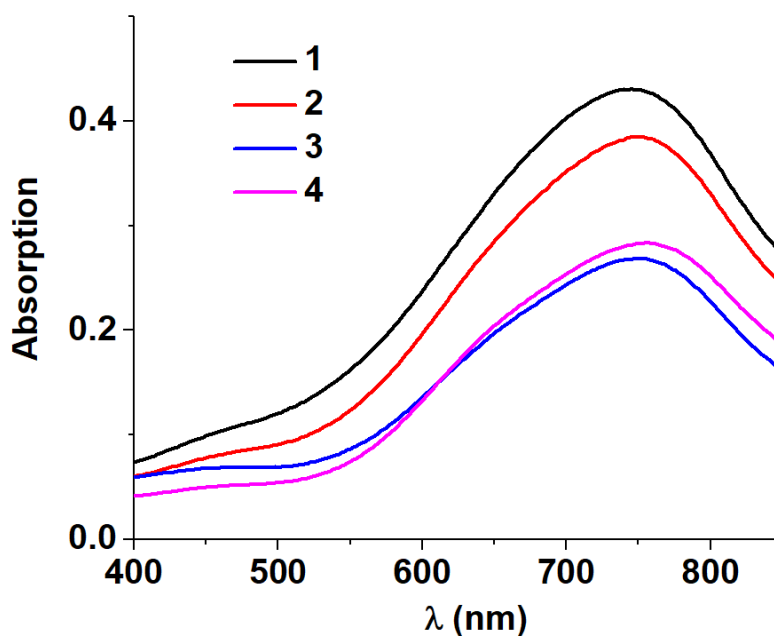
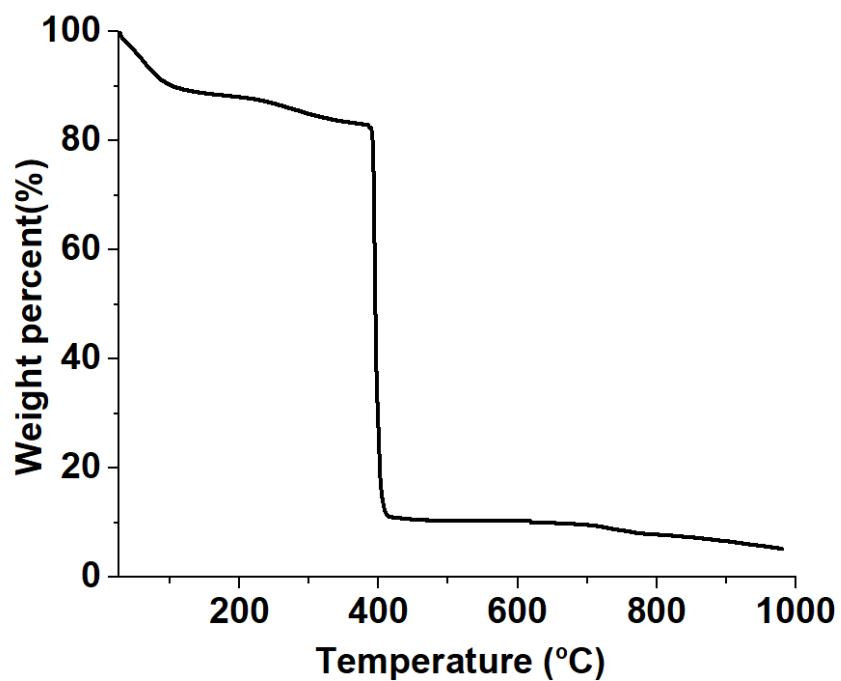
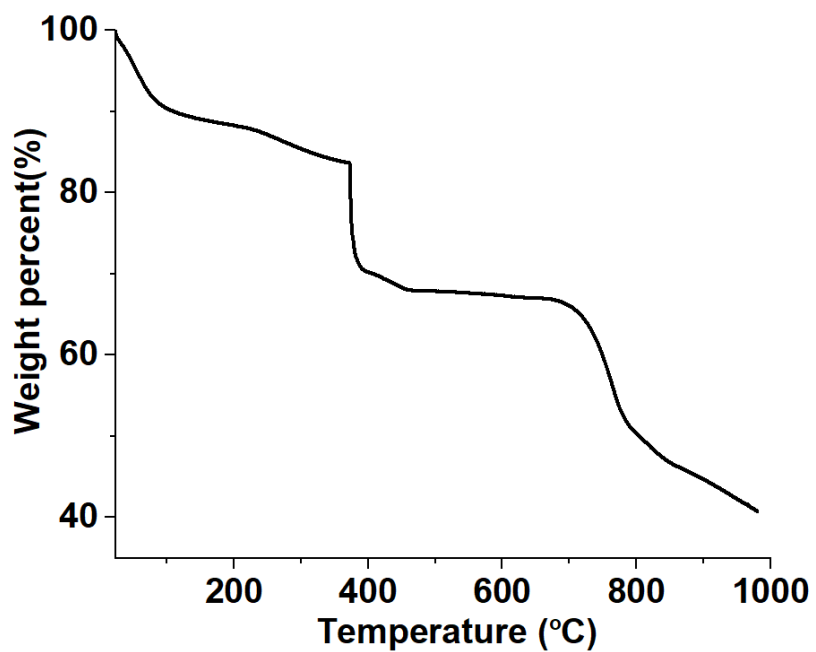


Figure S1 UV-vis-NIR spectra of **1-4** in water.



**Figure S2** TGA curve for compound 1. 11.90% weight loss from r.t. to 150 °C corresponds to ~160 H<sub>2</sub>O.



**Figure S3** TGA curve for compound 2. 11.40% weight loss from r.t. to 150 °C corresponds to ~195 H<sub>2</sub>O.

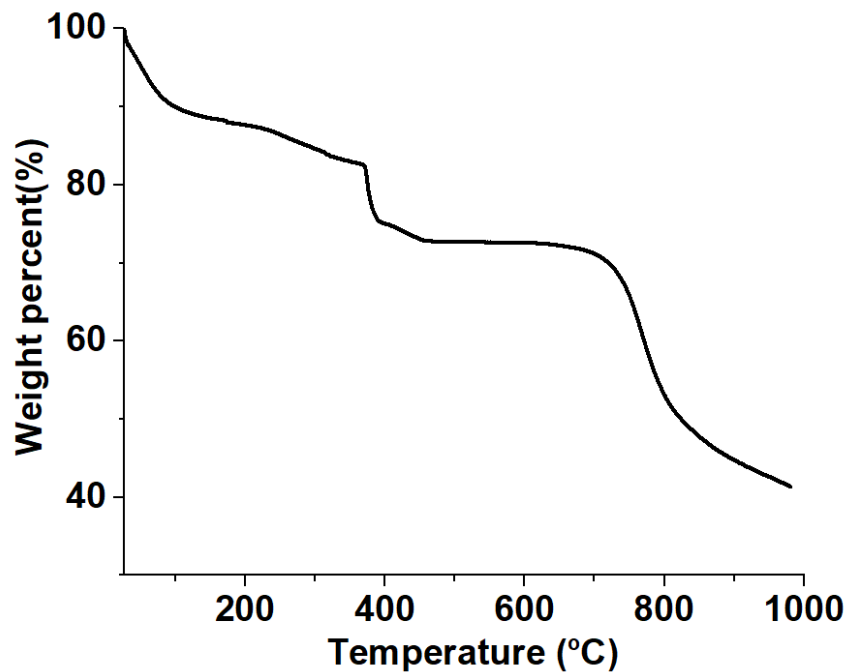


**Figure S4** TGA curve for compound 3. 11.60% weight loss from r.t. to 150 °C corresponds to ~195 H<sub>2</sub>O.

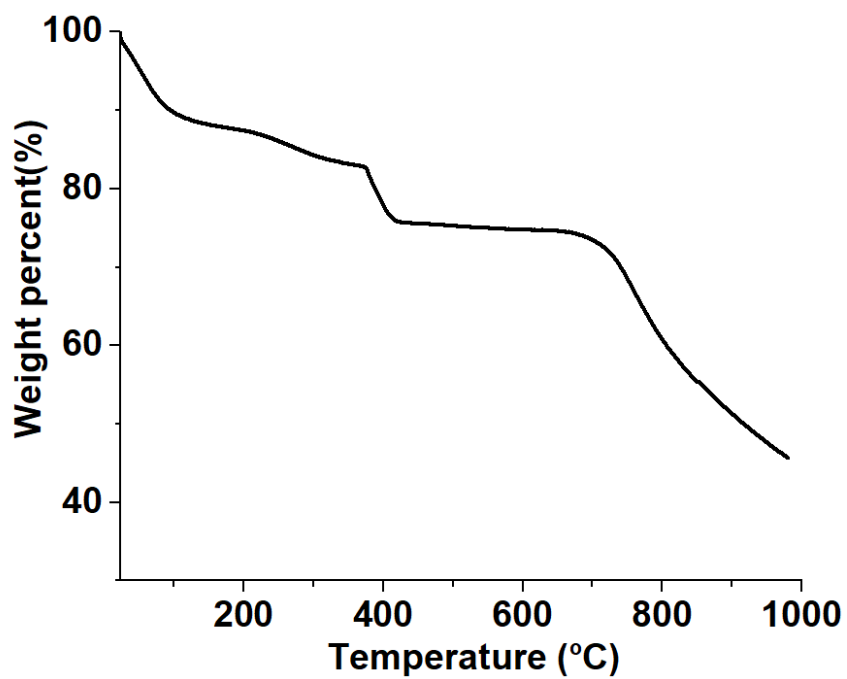
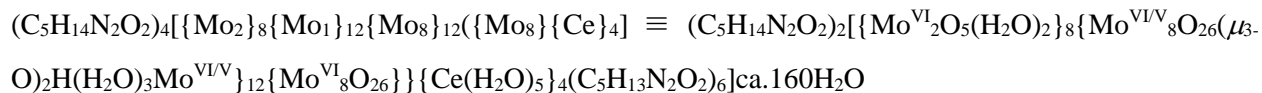


**Figure S5** TGA curve for compound 4. 11.90% weight loss from r.t. to 150 °C corresponds to ~410 H<sub>2</sub>O.

## Summary of structure analysis

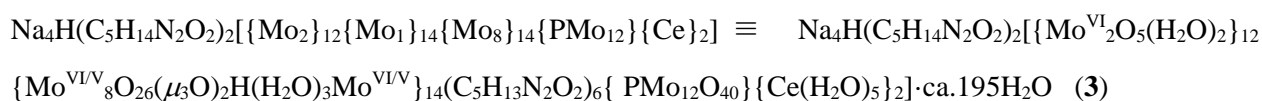
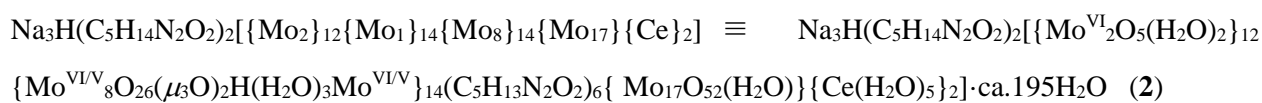
**Compound 1 :** Firstly, the overall reduction state of **1a** (24 electrons reduced) was confirmed using bond valence sum analysis. The formula of  $\{\text{Mo}_{124}\text{Ce}_4\}$  is calculated based upon the well-established lanthanide-doped Mo Blue. The framework of  $\{\text{Mo}_{124}\text{Ce}_4\}$  could be regarded 12 sets of  $\{\text{Mo}_{11}\}$ , of which four  $\{\text{Mo}_2\}$  units are replaced by 4  $[\text{Ce}(\text{H}_2\text{O})_5]^{3+}$ . The entrapped  $\{\text{Mo}_8\}$  is highly distorted with an occupancy of 0.5, and the formula is adopted from the classical  $\alpha$ - $\{\text{Mo}_8\}$  cluster with the formula of  $[\text{Mo}_8\text{O}_{26}]^{4-}$ . There are six doubly protonated L-orinithinate on **1a**. Accordingly, the overall charge of **1a** in **1** is -4. To balance the negative charge of **1a**, 2 doubly protonated L-orinithine are proposed as counterions for **1a**. Elemental analysis results confirm that the framework of **1a** consists of 128 Mo atoms and 4 Ce, which is consistent with single-crystal X-ray diffraction measurement. The amount of L-orinithine is deduced from C, H, N analysis and there are 8 L-orinithine in the structure of **1a** in total. Of these, six are located on the framework of **1a** while another two are guest molecules/counterions, as previously stated. TGA curve of **1** exhibits a total weight loss of 11.4% from r.t. to 150 °C, which corresponds to ~160 guest water molecules. Taking into consideration the information obtained from the above calculations, in addition to single-crystal X-ray diffraction, elemental analyses, bond valence sum analysis and TGA, it is possible to determine the overall building-block scheme and overall formula for **1** as:



**Compound 2-3 :** The formulae of **2** and **3** are determined in a similar manner to **1**. Firstly, the overall reduction state of **2** and **3** (28 electrons reduced) was confirmed using bond valence sum analysis (BVS) and compared with the archetypal  $\{\text{Mo}_{154}\}$ . Since the encapsulated  $\{\text{Mo}_{17}\}$  (**2**) and  $\{\text{PMo}_{12}\}$  (**3**) are highly distorted, accurate BVS analysis could not be obtained, however we assume that both clusters are not reduced and all the Mo centers adopt +6 oxidation states. The formula of  $\{\text{Mo}_{17}\}$  is deduced from the two  $\{\text{Mo}_{17}\}$  moieties contained in reported  $\{\text{Mo}_{36}\}$ , while the formula of  $\{\text{PMo}_{12}\}$  is assigned directly based on the  $\beta$ -Keggin. Note that the occupancy of  $\{\text{Mo}_{17}\}$  is 0.5 and  $\{\text{PMo}_{12}\}$  is 1. There are six doubly protonated L-orinithinate on **2a** and **3a**. In this way, we could determine the overall charge of **2a** in **2** as -8 and **3a** in **3** as -9. Elemental analysis results confirm that the framework of **2a** consists of 167 Mo atoms and 2 Ce, and **3a** consists of 162 Mo atoms, 2 Ce and 1 P, both of which are consistent with single-crystal X-ray diffraction measurements. To balance the negative charge of **2a** and **3a**, 3 sodium ions, 2 doubly protonated L-orinithine and 1 proton are proposed as counterions for **2a** and 4 sodium ions, 2 protonated L-orinithine and 1 proton are suggested for **3a**, based on the elemental analysis result of Na. The amount of L-orinithine is deduced from C, H, N analysis and there are 8 L-orinithine in the structure of **2a** and **3a** in total. Of these, six are

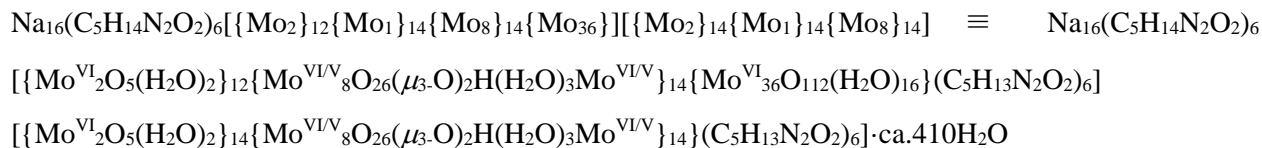
located on the framework of **2a** and **3a** while the remaining two are guest molecules/counterions. Finally, the TGA curves of **2** and **3** exhibit a total weight loss of 11.4 % and 11.6% from r.t. to 150 °C, respectively, which corresponds to ~195 guest water molecules.

The archetypal ring {Mo<sub>154</sub>} contains consists of 14 sets of three different building block types: {Mo<sub>8</sub>}, {Mo<sub>1</sub>} and {Mo<sub>2</sub>}. In a similar way, we can determine the composition of {Mo<sub>150</sub>} in **2a** as [{Mo<sub>2</sub>}]<sub>12</sub>{Mo<sub>1</sub>}]<sub>14</sub>{Mo<sub>8</sub>}]<sub>14</sub><sup>18-</sup> by deleting two {Mo<sub>2</sub>} units from {Mo<sub>154</sub>}. The positions of two further {Mo<sub>2</sub>} units are replaced by two [Ce(H<sub>2</sub>O)<sub>5</sub>]<sup>3+</sup> units. The formula of {Mo<sub>17</sub>} could be evaluated as [Mo<sub>17</sub>O<sub>52</sub>(H<sub>2</sub>O)]<sup>2-</sup>. Taking into consideration information obtained from the above calculations, in addition to single-crystal X-ray diffraction, elemental analyses, bond valence sum analysis and TGA, it is possible to determine the overall building-block scheme and overall formula for **2** and **3** as:



**Compound 4 :** The formula of **4** is determined in a similar manner to **1**. Firstly, the overall reduction state of **4a** (28 electrons reduced) was confirmed using bond valence sum analysis. The formula of the {Mo<sub>154</sub>} wheel (**4a<sub>2</sub>**) is adopted directly from archetypal ring {Mo<sub>154</sub>}, while {Mo<sub>150</sub>} (**4a<sub>1</sub>**) is determined by deleting two {Mo<sub>2</sub>} units from the same archetypal structure. The composition of entrapped {Mo<sub>36</sub>} is the same as the reported {Mo<sub>36</sub>}. There are six doubly protonated L-ornithinate on **4a<sub>1</sub>** and **4a<sub>2</sub>**. Accordingly, the overall charge of **4a<sub>1</sub>** and **4a<sub>2</sub>** in **4** is -28. Elemental analysis indicated the presence of 340 Mo on the frameworks of **4a<sub>1</sub>** and **4a<sub>2</sub>**. To balance the negative charge of **4a<sub>1</sub>** and **4a<sub>2</sub>**, 16 sodium ions and 6 doubly protonated L-ornithine are proposed as counterions. The number of L-ornithine present is deduced from C, H, N analysis, which indicates that there are in total 18 L-ornithine in the structure of **4**. Among them, six are located on the framework of **4a<sub>1</sub>** and **4a<sub>2</sub>**, respectively, while another six are guest molecules/counterions. TGA curve of **4** exhibits a total weight loss of 11.9% from r.t. to 150 °C, which corresponds to ~410 guest water molecules.

Taking into consideration the information obtained from the above calculations, in addition to single-crystal X-ray diffraction, elemental analyses, bond valence sum analysis and TGA, it is possible to determine the overall building-block scheme and overall formula for **4** as:



## 5. Crystallographic data and crystal structures of 1-4

**Table S2.** Crystal data and structure refinement for **1**

Identification code	<b>1</b>
Empirical formula	C40H558Ce4Mo128N16O625
Formula weight	24107.79
Temperature (K)	150(2)
Wavelength (Å)	0.71073
Crystal system	Orthorhombic
Space group	<i>P</i> 2 <sub>1</sub> 2 <sub>1</sub> 2 <sub>1</sub>
Unit cell dimensions	a = 38.114(3), α = 90° b = 39.898(3), β = 90° c = 47.356(3), γ = 90°
Volume (Å <sup>3</sup> ), Z	72014(8), 4
Density (calculated) (mg/m <sup>3</sup> )	2.224
Absorption coefficient (mm <sup>-1</sup> )	2.499
F(000)	46072
Crystal size (mm <sup>3</sup> )	0.100 x 0.050 x 0.050
θ range for data collection (°)	2.137 to 26.000
Limiting indices	-47<=h<=47, -49<=k<=49, -58<=l<=58
Reflections collected	918265
Independent reflections	141437 [R(int) = 0.0511]
Completeness to theta	25.242/ 99.9 %
Absorption correction	Empirical
Max. and min. transmission	0.745 and 0.675
Refinement method	Full-matrix least-squares on F <sup>2</sup>
Data / restraints / parameters	192434 / 46 / 8866
Goodness-of-fit on F <sup>2</sup>	1.172
Final R indices [I>2σ(I)]	R1 = 0.0693, wR2 = 0.1754
R indices (all data)	R1 = 0.0937, wR2 = 0.2150
Absolute structure parameter	0.005(3)
Largest diff. peak and hole (e.Å <sup>-3</sup> )	2.36 and -1.84

**Table S3.** Crystal data and structure refinement for **2**

Identification code	<b>2</b>
Empirical formula	C <sub>40</sub> H <sub>672</sub> Ce <sub>2</sub> Mo <sub>158.50</sub> N <sub>16</sub> Na <sub>3</sub> O <sub>770</sub>
Formula weight	29257.60
Temperature (K)	150(2)
Wavelength (Å)	0.71073
Crystal system	Orthorhombic
Space group	<i>Pbca</i>
Unit cell dimensions	a = 36.1134(15), $\alpha = 90^\circ$ b = 47.727(2), $\beta = 90^\circ$ c = 47.799(2), $\gamma = 90^\circ$
Volume (Å <sup>3</sup> ), Z	82387(6), 4
Density (calculated) (mg/m <sup>3</sup> )	2.359
Absorption coefficient (mm <sup>-1</sup> )	2.545
F(000)	55960
Crystal size (mm <sup>3</sup> )	0.100 x 0.050 x 0.050
$\theta$ range for data collection (°)	1.022 to 25.382
Limiting indices	-43 ≤ h ≤ 42, -56 ≤ k ≤ 57, -57 ≤ l ≤ 49
Reflections collected	557824
Independent reflections	75410 [R(int) = 0.0891]
Completeness to theta	25.242/ 99.9 %
Absorption correction	Empirical
Max. and min. transmission	0.7452 and 0.6056
Refinement method	Full-matrix least-squares on F <sup>2</sup>
Data / restraints / parameters	75410 / 30 / 3853
Goodness-of-fit on F <sup>2</sup>	1.245
Final R indices [I > 2σ(I)]	R1 = 0.0920, wR2 = 0.2063
R indices (all data)	R1 = 0.1473, wR2 = 0.2683
Largest diff. peak and hole (e.Å <sup>-3</sup> )	2.13 and -1.47

**Table S4.** Crystal data and structure refinement for **3**

Identification code	<b>3</b>
Empirical formula	C <sub>40</sub> H <sub>663</sub> Ce <sub>2</sub> Mo <sub>16</sub> N <sub>16</sub> Na <sub>4</sub> O <sub>779</sub> P
Formula weight	29782.28
Temperature (K)	150(2)
Wavelength (Å)	0.71073
Crystal system	Orthorhombic
Space group	<i>Pbca</i>
Unit cell dimensions	a = 47.732(4), $\alpha = 90^\circ$ b = 36.019(3), $\beta = 90^\circ$ c = 47.894(4), $\gamma = 90^\circ$
Volume (Å <sup>3</sup> ), Z	82343(12), 4
Density (calculated) (mg/m <sup>3</sup> )	2.402
Absorption coefficient (mm <sup>-1</sup> )	2.602
F(000)	56904
Crystal size (mm <sup>3</sup> )	0.100 x 0.050 x 0.050
$\theta$ range for data collection (°)	1.107 to 25.204
Limiting indices	$57 \leq h \leq 57$ , $-43 \leq k \leq 40$ , $-44 \leq l \leq 57$
Reflections collected	565504
Independent reflections	73917 [R(int) = 0.0900]
Completeness to theta	25.204 / 99.6%
Absorption correction	Empirical
Max. and min. transmission	0.745 and 0.597
Refinement method	Full-matrix least-squares on F <sup>2</sup>
Data / restraints / parameters	73917 / 24 / 4076
Goodness-of-fit on F <sup>2</sup>	1.255
Final R indices [I > 2 $\sigma$ (I)]	R1 = 0.0850, wR2 = 0.1821
R indices (all data)	R1 = 0.1217, wR2 = 0.2115
Largest diff. peak and hole (e.Å <sup>-3</sup> )	2.39 and -1.86

**Table S5.** Crystal data and structure refinement for **4**

Identification code	<b>4</b>
Empirical formula	C <sub>90</sub> H <sub>1344</sub> Mo <sub>340</sub> N <sub>36</sub> Na <sub>16</sub> O <sub>1600</sub>
Formula weight	61527.37
Temperature (K)	150(2)
Wavelength (Å)	0.71073
Crystal system	Triclinic
Space group	<i>P</i> -1
Unit cell dimensions	a = 27.367(4), $\alpha$ = 98.600(7) ° b = 27.663(4), $\beta$ = 98.834(7) ° c = 63.835(8), $\gamma$ = 94.197(7) °
Volume (Å <sup>3</sup> ), Z	46987(11), 1
Density (calculated) (mg/m <sup>3</sup> )	2.174
Absorption coefficient (mm <sup>-1</sup> )	2.291
F(000)	29392
Crystal size (mm <sup>3</sup> )	0.100 x 0.050 x 0.050
$\theta$ range for data collection (°)	0.766 to 24.831
Limiting indices	-32 ≤ h ≤ 31, -32 ≤ k ≤ 32, -74 ≤ l ≤ 68
Reflections collected	493374
Independent reflections	156210 [R(int) = 0.1206]
Completeness to theta	24.831/ 96.2%
Absorption correction	Empirical
Max. and min. transmission	0.745 and 0.488
Refinement method	Full-matrix least-squares on F <sup>2</sup>
Data / restraints / parameters	156210 / 190 / 7678
Goodness-of-fit on F <sup>2</sup>	1.079
Final R indices [I > 2σ(I)]	R1 = 0.1150, wR2 = 0.2793
R indices (all data)	R1 = 0.1921, wR2 = 0.3416
Largest diff. peak and hole (e.Å <sup>-3</sup> )	2.05 and -2.02

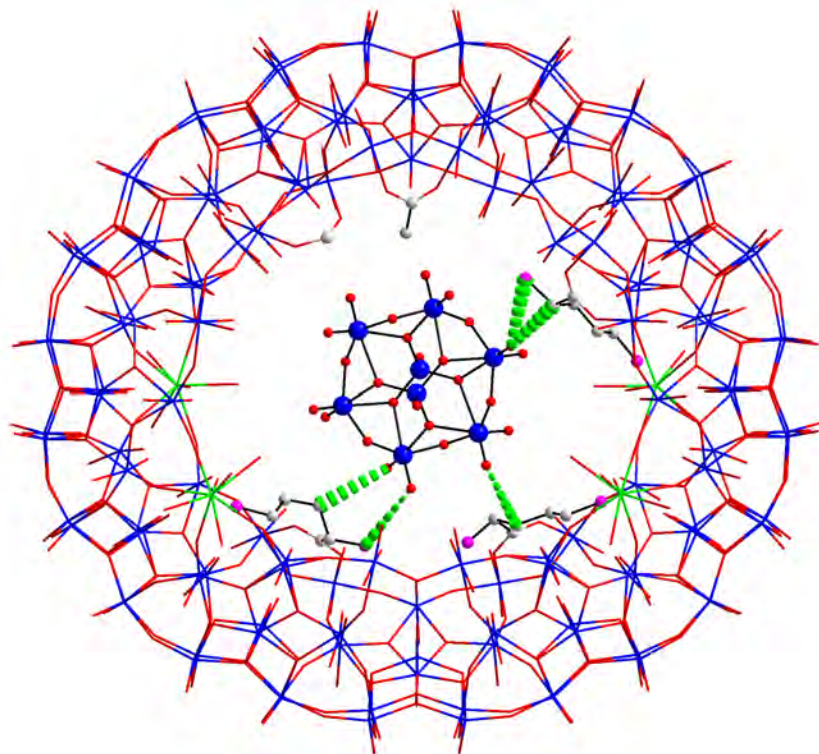


**Figure S6.** Hydrogen bonds formed between {Mo<sub>8</sub>} and L-ornithine in **1a**. Mo, blue; Ce, green; O, red; C, gray; N, pink.

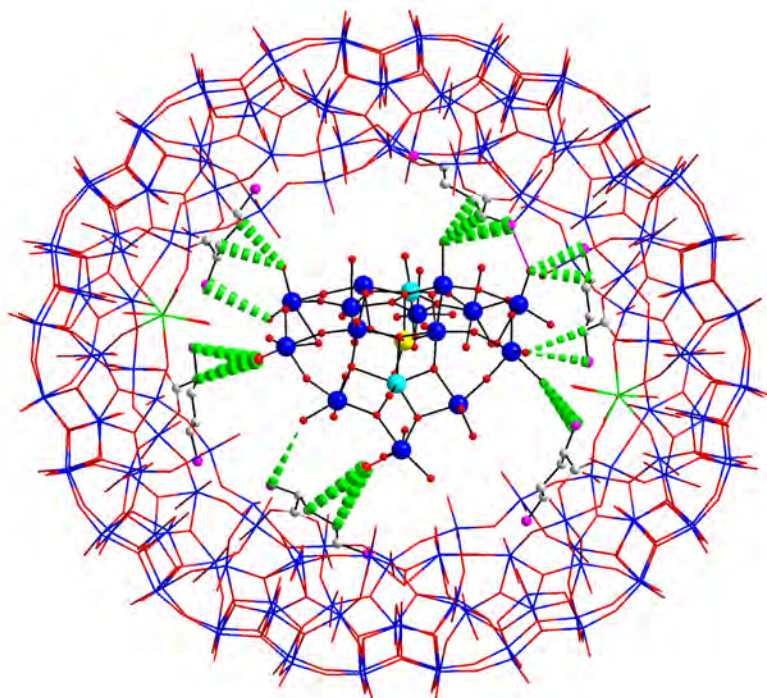


**Figure S7.** Hydrogen bonds formed between {Mo<sub>17</sub>} and L-ornithine in **2a**. Mo, blue; Ce, green; O, red; C, gray; N, pink.

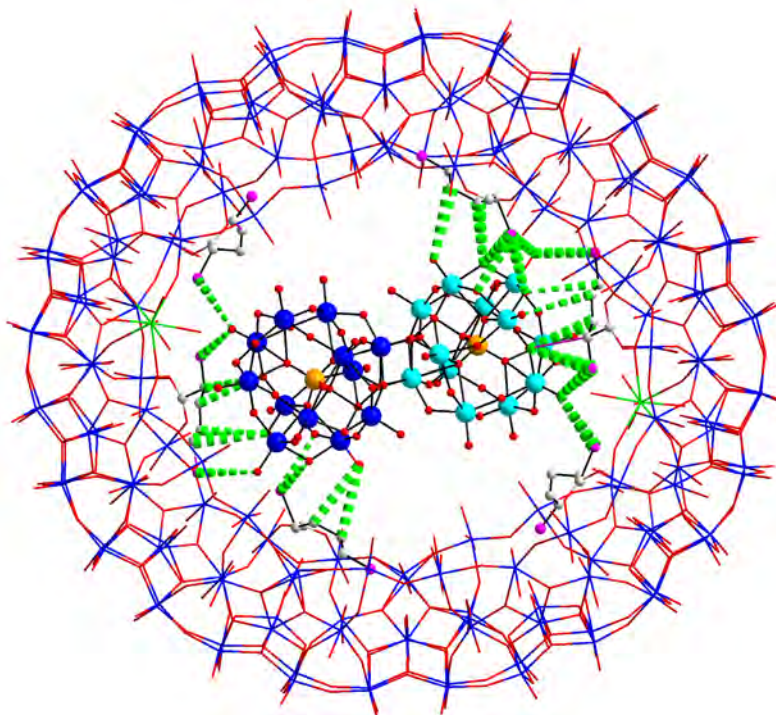


**Figure S8.** Hydrogen bonds formed between  $\{\text{PMo}_{12}\}$  and L-ornithine in **3a**. Mo, blue; Ce, green; O, red; C, gray; N, pink.

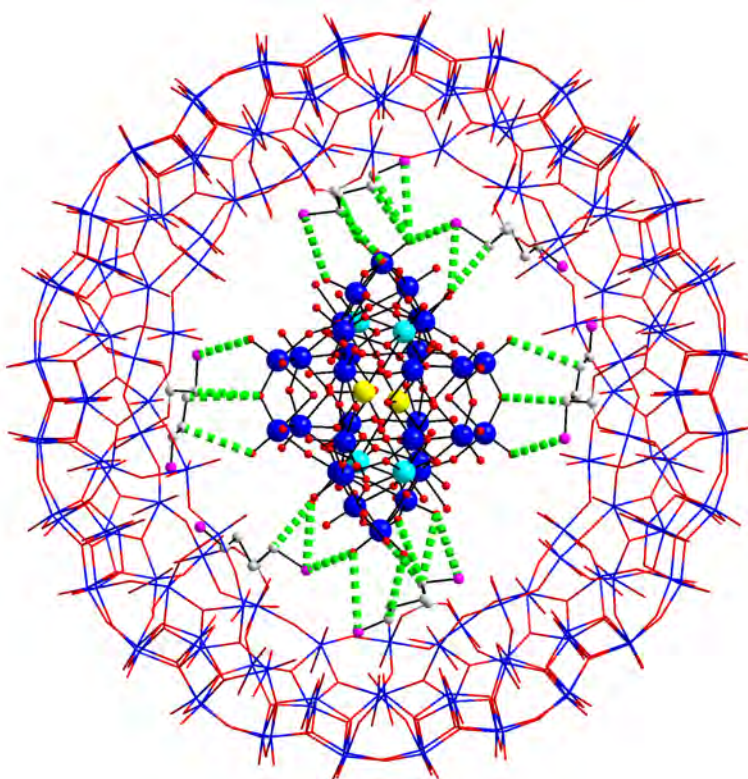


**Figure S9.** Hydrogen bonds formed between  $\{\text{Mo}_{36}\}$  and L-ornithine in **4a1**. Mo, blue; Ce, green; O, red; C, gray; N, pink.

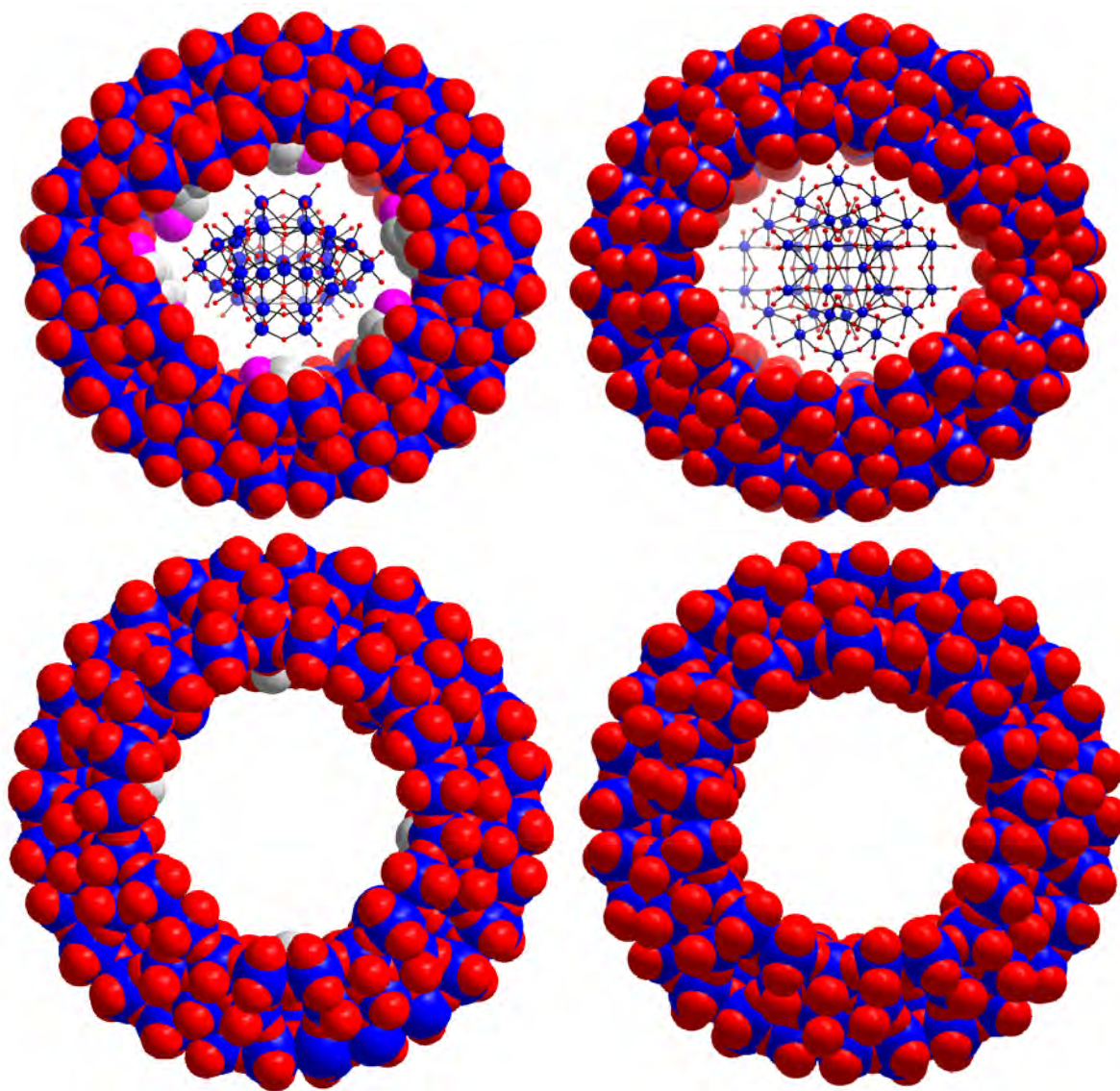


**Figure S10.** Space filling mode of **4a<sub>1</sub>** (top left), **{Mo<sub>36</sub>}@{Mo<sub>150</sub>}** (top right), **4a<sub>2</sub>** (bottom left) and **{Mo<sub>154</sub>}** (bottom right). The **{Mo<sub>36</sub>}** in **4a<sub>1</sub>** and **{Mo<sub>36</sub>}@{Mo<sub>150</sub>}** is presented in ball and stick mode. Mo, blue; Ce, green; O, red; C, gray; N, pink.

## 5. Time resolved $^{31}\text{P}$ NMR study of the templated assembly of **3**

The time-resolved  $^{31}\text{P}$  NMR study is performed during the scaledown synthesis of **3**:

L-ornithine.HCl (2.87 mg, 0.017 mmol),  $\text{CeCl}_3 \cdot 7\text{H}_2\text{O}$  (7.5 mg, 0.02 mmol),  $\text{H}_3\text{PMo}_{12}\text{O}_{40} \cdot n\text{H}_2\text{O}$  (8 mg, 0.0044 mmol) and  $\text{N}_2\text{H}_4 \cdot 2\text{HCl}$  (1.5 mg, 0.014 mmol) were added to a solution of  $\text{Na}_2\text{MoO}_4 \cdot 2\text{H}_2\text{O}$  (0.1 g, 0.413 mmol) in mixture of water (5 mL) and  $\text{D}_2\text{O}$  (1 mL). The mixture was then acidified with 2M HCl to pH  $\sim 1.0$  and transferred to NMR tube equipped with an inserted tube that contains phenyl phosphonic acid (2 mg) in  $\text{D}_2\text{O}$  as external reference. The NMR tube was then heated at  $70^\circ\text{C}$  for 1 h, and the  $^{31}\text{P}$  NMR spectrum was recorded every 10 min (Figure S10a and S10b). **Note:** the chemical shift of phenyl phosphonic acid is at 16.325 ppm.

To make a comparison, 2.5 mg  $\text{H}_3\text{PMo}_{12}\text{O}_{40} \cdot n\text{H}_2\text{O}$  was used for  $^{31}\text{P}$  NMR study in the same way (Figure S10c and S10d). Since the theoretical amount of  $\text{H}_3\text{PMo}_{12}\text{O}_{40} \cdot n\text{H}_2\text{O}$  that is required to template the self-assembly of all the  $\text{Na}_2\text{MoO}_4 \cdot 2\text{H}_2\text{O}$  (0.1 g) into  $\{\text{Mo}_{150}\text{Ce}_2\}$  (0.0027 mmol) is around 5 mg. In principle, 2.5 mg  $\text{H}_3\text{PMo}_{12}\text{O}_{40} \cdot n\text{H}_2\text{O}$  will be completely consumed as template while excess  $\text{H}_3\text{PMo}_{12}\text{O}_{40} \cdot n\text{H}_2\text{O}$  will remain in solution when 8 mg is used. Therefore, the  $^{31}\text{P}$  NMR signal corresponding to  $\text{H}_3\text{PMo}_{12}\text{O}_{40} \cdot n\text{H}_2\text{O}$  should be still observed after the reaction when using 8 mg  $\text{H}_3\text{PMo}_{12}\text{O}_{40} \cdot n\text{H}_2\text{O}$  whereas no signal should be seen in the case of 2.5 mg  $\text{H}_3\text{PMo}_{12}\text{O}_{40} \cdot n\text{H}_2\text{O}$  (Figure S11a-d).

The  $^{31}\text{P}$  NMR spectrum of  $\text{H}_3\text{PMo}_{12}\text{O}_{40} \cdot n\text{H}_2\text{O}$   $\{\text{PMo}_{12}\}$  (Figure S11e) was recorded by dissolving 4 mg  $\text{H}_3\text{PMo}_{12}\text{O}_{40} \cdot n\text{H}_2\text{O}$  in 0.5 mL  $\text{D}_2\text{O}$  with pH adjusted to 1.0 by 2M HCl. In the same way, phenyl phosphonic acid (2 mg) was used as external reference.

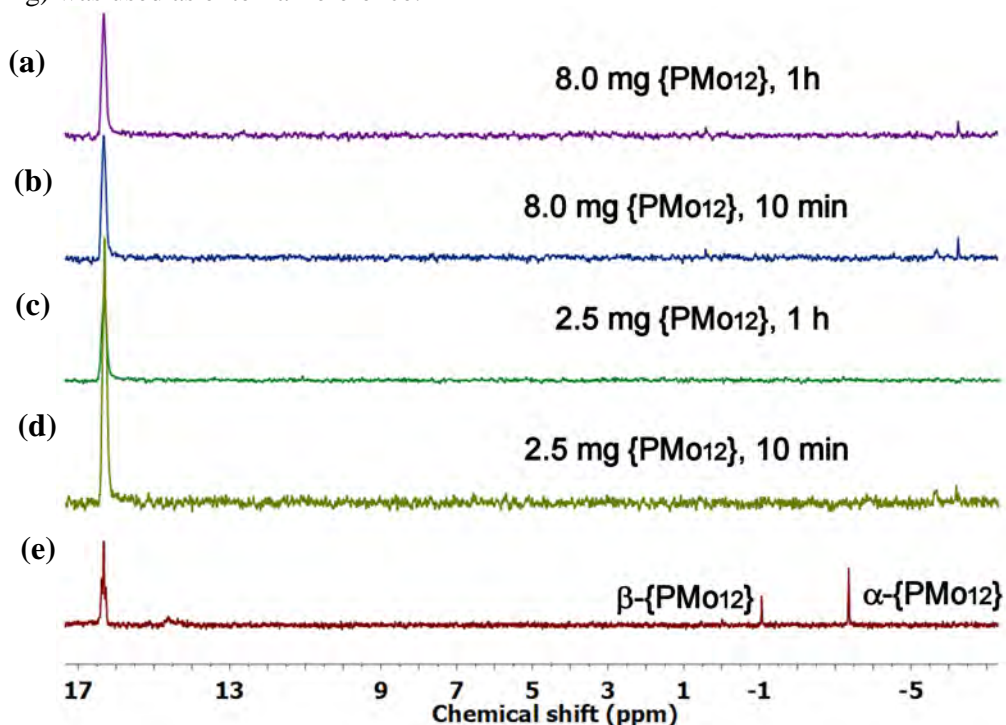


**Figure S11.**  $^{31}\text{P}$  NMR study of the templated assembly of **3**. From up to bottom, (a) 8.0 mg  $\{\text{PMo}_{12}\}$  reacting for 1 h; (b) 8.0 mg  $\{\text{PMo}_{12}\}$  reacting for 10 min; (c) 2.5 mg  $\{\text{PMo}_{12}\}$  reacting for 1 h; (d) 2.5 mg  $\{\text{PMo}_{12}\}$  reacting for 10 min; (e) 4 mg  $\{\text{PMo}_{12}\}$ . The signal at 16.325 ppm corresponds to the external reference, phenyl phosphonic acid.

## 6. Reference

1. G. Sheldrick, *Acta Crystallographica Section A*, **1990**, *46*, 467-473.
2. G. Sheldrick, *Acta Crystallographica Section A*, **2008**, *64*, 112-122.
3. L. Farrugia, *J. Appl. Crystallogr.*, **1999**, *32*, 837-838.
4. a) A. Müller, E. Krickemeyer, H. Bögge, M. Schmidtman, C. Beugholt, S. K. Das, F. Peters, *Chem. Eur. J.* **1999**, *5*, 1496-1502; b) A. Müller, C. Serain, *Acc. Chem. Res.* **2000**, *33*, 2-10.
5. I. D. Brown, In *Structure and Bonding in Crystals*, Vol. II (Ed.: M.O'Keefe, A. Navrotsky, Academic Press, New York, 1981), p. 1.